Available online at www.sciencedirect.com
ScienceDirect
Journal of Power Sources 173 (2007) 965–971
JOURNAL OF POWER SOURCES
www.elsevier.com/locate/jpowsour

Microwave plasma chemical vapor deposition of nano-structured Sn/C composite thin-film anodes for Li-ion batteries

M. Marcinek, L.J. Hardwick, T.J. Richardson, X. Song, R. Kostecki *

Environmental Energy Technologies Division, Lawrence Berkeley National Laboratory, Berkeley, CA 94720, USA

Received 17 July 2007; received in revised form 23 August 2007; accepted 30 August 2007
Available online 4 September 2007

Abstract

A novel synthesis method of thin-film composite Sn/C anodes for lithium batteries is reported. Thin layers of graphitic carbon decorated with uniformly distributed Sn nanoparticles were synthesized from a solid organic precursor Sn(IV) *tert*-butoxide by a one-step microwave plasma chemical vapor deposition (MPCVD). The thin-film Sn/C electrodes were electrochemically tested in lithium half cells and produced a reversible capacity of 423 and 297 mAh g^{-1} at *C*/25 and 5*C* discharge rates, respectively. A long-term cycling of the Sn/C nanocomposite anodes showed 40% capacity loss after 500 cycles at 1*C* rate.

Keywords: Sn/C; Lithium batteries; Anode; Plasma; Microwave

1. Introduction

The development of new cathode and anode materials meets an extensive market demand for an advanced generation of lithium batteries with greater energy densities and improved cycle life properties. In most of the conventional Li-ion systems, graphitic anodes are used as an intercalation host for lithium to form LiC_6, which corresponds to a charge capacity of 372 mAh g^{-1}. An extensive number of experimental approaches have been proposed to increase the anode's electrochemical capacity [1,2]. Several modifications of carbons [3–7], nitrides [8,9], oxides [10–14] or alloying of lithium with metals such an Si [15], Sn [16] and Al [17] were proposed. Among them, tin seems to be particularly attractive since it easily and reversibly alloys with Li atoms at potentials <1.1 V versus Li. Other attractive properties of tin include fast Li diffusion, better safety, easy mechanical processing, and crucially, a high gravimetric 993 mAh g^{-1} and volumetric 7262 mAh cm^{-3} specific theoretical capacities [18–20].

The first commercially available amorphous tin-based composite anode was introduced to the market by Sony in 2006 [21], followed by detailed studies of $Sn_{0.34}Co_{0.19}C_{0.47}$ systems by Dahn and co-workers [22], which demonstrated the capabilities of these electrodes in high-energy Li-ion systems.

Unfortunately one of the major obstacles to the use of pure tin as an active material is its large volumetric expansion during the alloying with lithium, which causes cracking and mechanical disintegration of Sn particles. Loss of mechanical and electronic integrity of the active material leads to severe degradation of the composite anode upon cycling and dramatically shortens the cycle life of the electrode. One proposed resolution to overcome this problem is to use tin oxide as a soft matrix to ameliorate the expansion of the metal [23–27]. Alternative solutions include the use of tin alloys [28–41] and other tin-based composite materials such as $LiSn_2(PO_4)_3$ [20]. Minimizing the thickness of the electrode, as well as reducing the particle size [42] and uniform particle distribution within the supporting matrix [43], can help accommodate the mechanical stress induced in the crystalline lattice of Li_xSn. This can have the effect of preventing particle agglomeration and improving long-term electrochemical performance.

Sn, SnO_2 and Sn-based alloy composites with graphite [44–47], amorphous carbon [48,49] or carbon nanotubes [50] used as a mechanical support and conductive matrix for tin-based active material particles also offer a unique opportunity to combine the stable cyclability of the carbon with the high-

* Corresponding author. Tel.: +1 510 486 6002; fax: +1 510 486 7303.
E-mail address: r_kostecki@lbl.gov (R. Kostecki).

0378-7753/$ – see front matter © 2007 Elsevier B.V. All rights reserved.
doi:10.1016/j.jpowsour.2007.08.084

storage capacity of tin-based materials. Fabrication techniques of nano-structured Sn, SnO_2 and carbon/tin composites include autocatalytic deposition [44], ball-milling [41,45,51], chemical reduction [46,50], electrodeposition [47], hydrolysis [48], pyrolysis [49] sputtering [52], plasma laser deposition (PLD) [53], sol–gel techniques [54], partial reduction [55], precipitation [56], sonochemical methods [57], and vapor deposition [58]. However, these processes often involve several time consuming steps and offer only limited control of the particle size and distribution. Moreover, typical Sn, SnO_2 and Sn-based alloy anodes are prepared by using the conventional lamination method which involves slurry preparation (grinding, mixing with binders and solvents), laminating, drying, heating, etc.

In this work we present a new, one-step microwave plasma chemical vapor deposition (MPCVD) of nano-dispersed tin–carbon composite thin-film anodes for Li-ion batteries. This experimental approach provides an easy, fast and inexpensive method for the direct formation of thin films of uniformly distributed ultra-fine grains of metal within an electronically conductive graphitic matrix [59].

2. Experimental

A detailed description of the experimental setup can be found in Ref. [59]. The Sn/C film can be produced on various types of conductive and non-conductive substrate materials from a tin-based organic salt precursor without using stabilizers or reducing agents. In this work, a small amount (∼2 mg) of the Sn(IV) *tert*-butoxide $Sn(OC(CH_3)_3)_4$ (Sigma–Aldrich) organic precursor was placed ∼5 mm from a substrate (∼1 cm^2 piece of Cu foil or glass) in a Pyrex glass tube reactor. The deposition process was carried out for 6 s at 1200 W microwave radiation power, which produced a ∼5 μm thick nanocomposite Sn/C film. The qualitative analysis of the Sn/C films by inductively coupled plasma (Perkin-Elmer Optima 5300DV ICP-OES) spectroscopy produced a C/Sn mass ratio of 2.5:1, i.e., much higher than in the Sn(IV) *tert*-butoxide (1.6:1). The thickness and composition of the film were reproducible and not dependent on the type of substrate.

The structure of carbon in composite Sn/C films was analyzed by Raman microscopy (Labram, ISA Group Horiba) with a laser excitation wavelength of either 632.8 or 488 nm, at 1 mW power at the sample surface. The morphology of the thin film and the nanoparticle size were characterized by transmission electron microscopy (TEM, model JEOL 200CX), and scanning electron microscopy (SEM, model Hitachi S-4300 SE/N. An X-ray powder diffraction pattern of a Sn/C thin-film deposited on a glass substrate was obtained using a Philips X-Pert PRO diffractometer operating in Bragg–Brentano mode with Cu Kα radiation. The 2θ step size was 0.017° and counting time 400 s per step. The whole pattern fitting process was carried out using Powdercell software [60].

Electrochemical characterization was conducted in a He-filled glove box (VAC Inc.) with a model 273A Princeton Applied Research electrochemical station. The tests were carried out in a three-electrode cell equipped with Li foil reference and counter electrodes and filled with the 1.0 M $LiPF_6$ EC/DMC (1:1 w/w) electrolyte. The cyclic voltammetry measurements were performed at 0.1 mV s^{-1}.

3. Results

Fig. 1 shows the X-ray diffraction pattern of the 5 μm thick Sn/C film. The low intensity of the pattern is due primarily to the high porosity of the film. The only phase clearly observed is elemental Sn ($I4_1/amd$). The refined tetragonal lattice parameters a_0 and c_0 are 5.86 and 3.19 Å, respectively. These are slightly larger than the bulk values 5.831 and 3.176 Å, as is common for small particles. The average Sn crystallite size calculated using the Scherrer equation was ∼15 nm.

SEM images (Fig. 2a and b) of the surface morphology and cross-section of the Sn/C composite layer display a uniform thin film of fairly constant thickness ca. 5–6 μm. The morphology of this porous film is consistent in the film bulk and at the surface. The film is made up of large 300–600 nm agglomerates. According to supplementary observations (data not shown here) the aggregates consist of small disoriented crystallites. The domains form an interconnected network with a micro- and nano-porous "lava rock" structure. The EDX spectrum of the Sn/C film (Fig. 2c) shows strong signals characteristics for L tin family at (SnL_l) 3.156, (Sn $L\alpha_2$, Sn $L\alpha_1$) 3.414, (Sn $L\beta_1$, Sn $L\beta_4$, Sn $L\beta_3$) 3.600, (Sn $L\beta_2$) 3.929, (Sn $L\gamma_1$) 4.07 keV, carbon (C Kα) 0.27 keV and copper substrate (Cu $L\alpha_1$) 0.94 keV. A small contribution from oxygen at (OKα) 0.53 keV suggests the presence of tin oxide impurities in the layer [61].

The typical Raman spectra of a C/Sn thin-film recorded at two excitation wavelengths 632.8 and 488 nm are displayed in Fig. 3. The spectrum recorded at 632.8 nm wavelength exhibits two intense peaks assigned as the G- and D-band at 1583 and 1323 cm^{-1} that correspond to the E_{2g} and A_{1g} carbon vibration modes, respectively [62]. The D-band is associated with the break in symmetry occurring at the edges of the graphite sheets. A shoulder at 1620 cm^{-1}, known as the D'-band, is also attributed to discontinuity and disorder within graphene planes, but the exact nature of this peak is still under dispute [63–65].

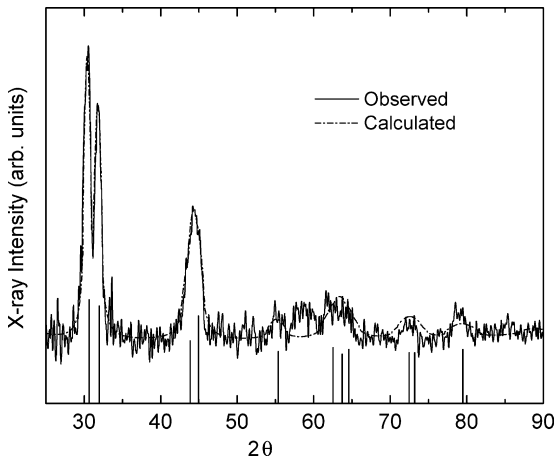

Fig. 1. X-ray diffraction pattern of Sn/C composite film on glass. Vertical markers represent peak positions for bulk tetragonal Sn (PDF Reference Pattern 4-673, International Centre for Diffraction Data).

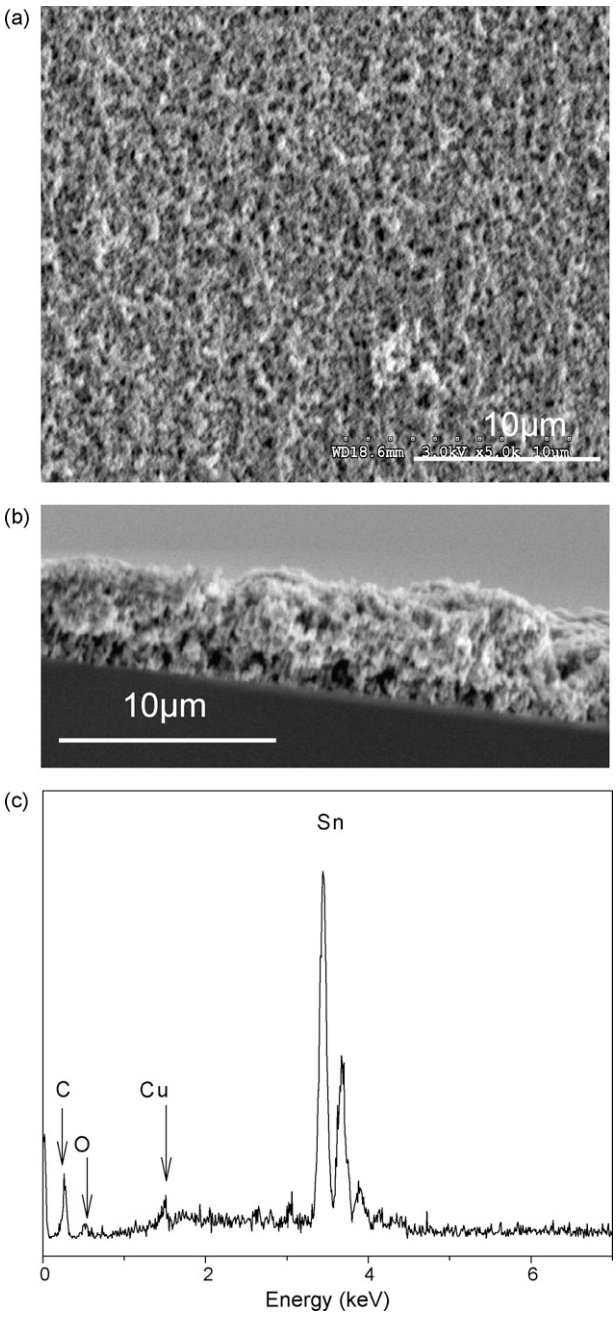

Fig. 2. SEM micrographs of the surface (a), cross-section (b), and the corresponding EDX spectrum (c) of the Sn/C composite thin-film deposited by MPCVD on Cu foil.

The presence of strong graphite G and D modes along with the absence of a sharp diamond Raman peak at ~1330 cm^{-1} in the Raman spectra suggests that the C/Sn films consist mainly of a sp^2-coordinated carbon phase. The location of the G-band, which is typical for graphite and carbon blacks, is quite insensitive to the excitation wavelength. However, the observed shift of the D-band position from 1323 to 1344 cm^{-1} and the decreased peak intensity as the laser excitation is varied from 632.8 to 488 nm represents typical spectral behavior of nano-crystalline graphite with a high degree of disorder [66,67].

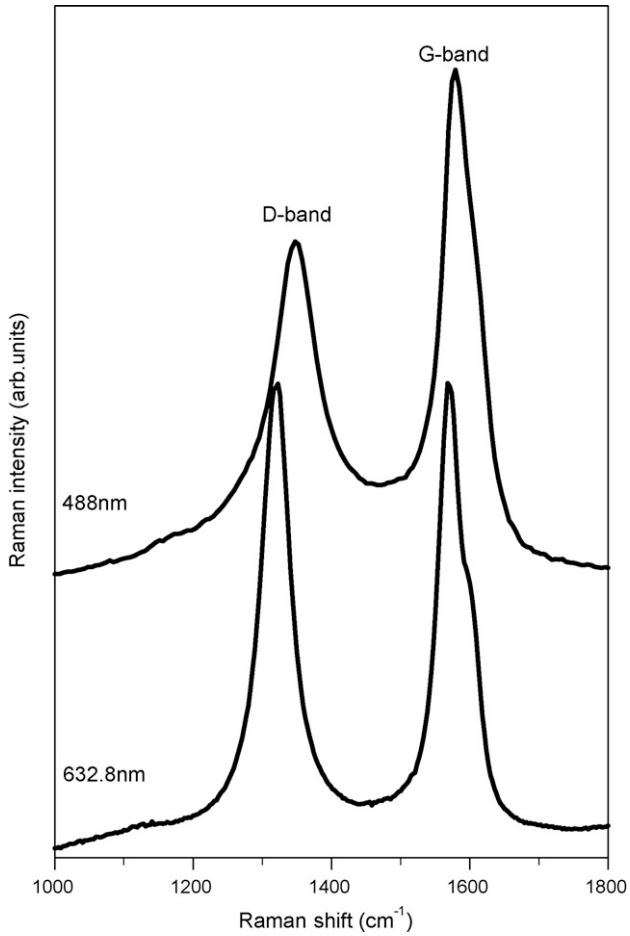

Fig. 3. Micro-Raman spectra of the Sn/C composite film recorded at 488 and 632.8 nm excitation wavelength.

TEM imaging was used to investigate the size and distribution of tin particles as well as the local structure of carbon in the Sn/C film. The dark-field TEM picture of the Sn/C composite is shown in Fig. 4a. The dark-field technique allows clear observation of particle morphology and the distribution of Sn on the surface of the Sn/C deposit. The dark contrast area is attributed to carbon, whereas light contrast spots represent Sn nanoparticles. The images show a remarkably uniform and fine dispersion of tin in the C/Sn composite. To determine the Sn particle size distribution in the Sn/C film, one hundred randomly selected Sn particles from the magnified TEM images were measured. The statistical representation of the Sn particle size distribution is displayed in Fig. 4b. The particle size distribution is very narrow; the calculated average size of Sn particles (ca. 2.75 nm) is noticeably smaller than the average particle size estimated from the X-ray data. The discrepancy between XRD and TEM particle sizes could be due to the presence of a small number of larger particles that contribute strongly to the XRD pattern. While they may represent a small fraction of the particles, they could represent a significant fraction of the mass of Sn.

The HRTEM image of the Sn/C agglomerate (Fig. 5) reveals a few 1–5 nm Sn particles (dark areas) that are fully embedded in partially graphitized, carbonaceous material. The presence of

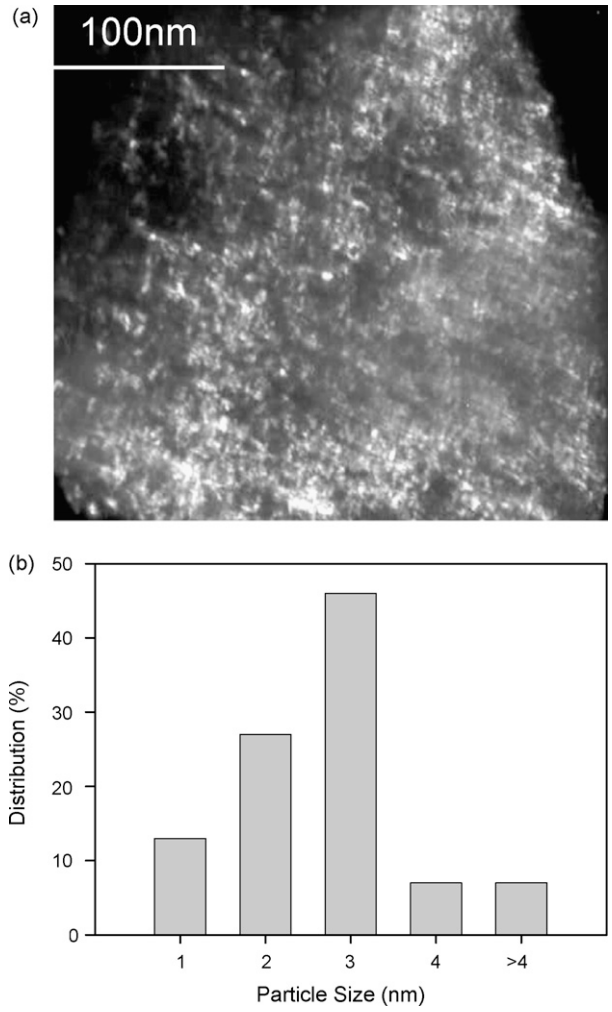

Fig. 4. (a) Dark-field TEM image of the Sn/C composite deposited by MPCVD and (b) diagram of Sn particle size distribution in the Sn/C composite.

nano-crystalline tin particles was confirmed by their electron diffraction patterns (not shown here). Interestingly, the carbon shows relatively large ca. 10–15 nm well-organized graphene domains in the bulk of the agglomerate as well as in locations

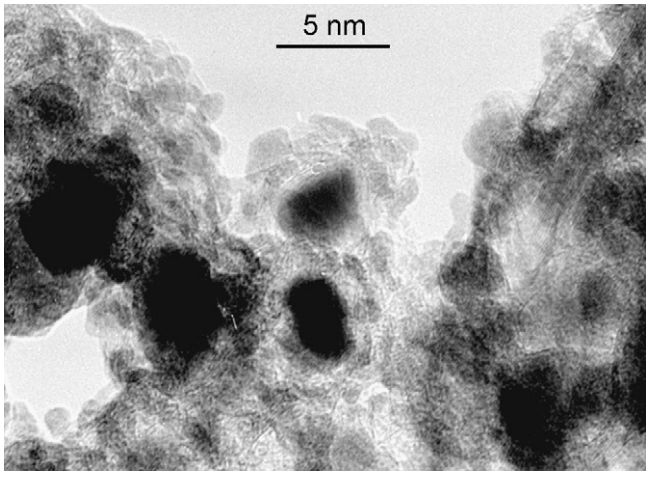

Fig. 5. HRTEM image of the Sn/C nanocomposite synthesized by MPCVD.

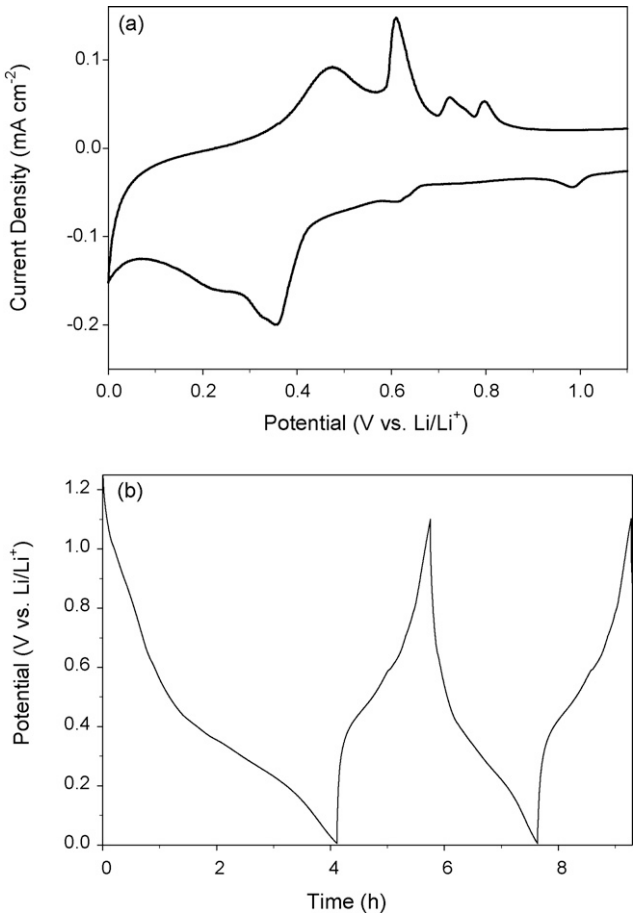

Fig. 6. (a) First CV scan of the Sn/C nanocomposite anode. Scan speed rate was 0.1 mV s^{-1} and (b) first two galvanostatic cycles of the Sn/C electrode at 1*C* rate.

adjacent to the Sn particles. It also displays regions where shorter layers of irregular shape prevail, which are typical of carbon blacks [68].

The thin-film Sn/C anode was characterized by cyclic voltammetry (CV) in the 1.0 M $LiPF_6$ EC/DMC (1:1 w/w) electrolyte at 0.1 mV s^{-1} scan rate (Fig. 6a). The CV profile is typical for tin, tin-based alloys or SnO_2 composites after several cycles where the Sn material is formed from tin oxide reaction with lithium in the first cycle. A weak cathodic peak at 0.98 V occurs only during the first scan and may be attributed to the irreversible reduction of the tin oxide impurities or the formation of the SEI layer. The peak at 0.65 V is usually attributed to early stages (Li_xSn, $x < 1$) of the Li–Sn alloying process. The large and broad cathodic peak at 0.37 V corresponds to the formation of highly lithiated phases, i.e., $Li_{4.4}Sn$, $Li_{2.33}Sn$. The anodic scan exhibits four distinct peaks at 0.48, 0.62, 0.73, and 0.8 V, which correspond to the delithiation of $Li_{4.4}Sn$, $Li_{2.33}Sn$, LiSn, and $Li_{0.4}Sn$ phases, respectively [28].

The Sn/C thin-film anodes display a relatively large reversible discharge capacity of ca. 440 mAh g^{-1} (calculated for the total mass of the Sn/C layer). Interestingly, no contribution to reversible capacity from the carbon support at potentials <0.25 V was observed unless the Sn/C anode was polarized at 0 V for a prolonged period of time (not shown here). The

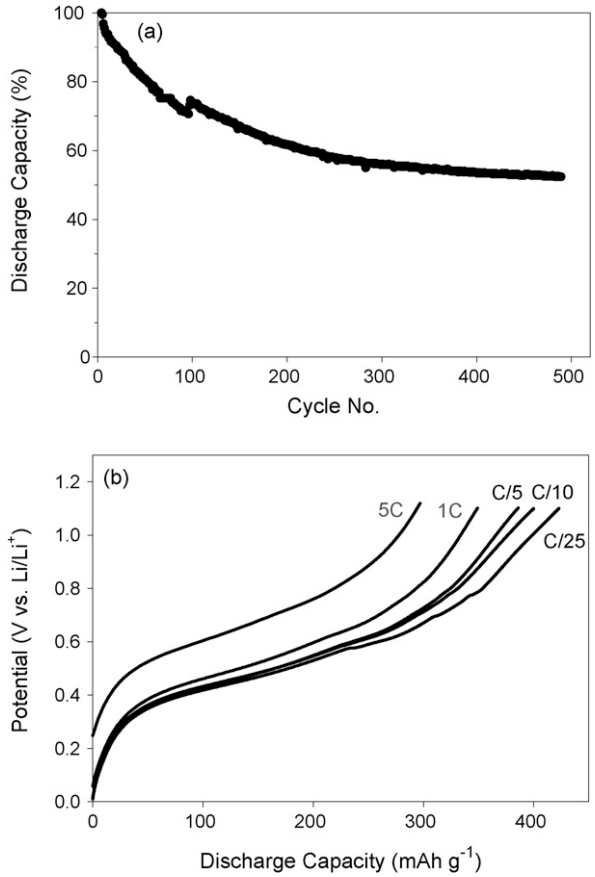

Fig. 7. (a) Discharge capacity of the Sn/C thin-film nanocomposite anode during a long-term cycling at room temperature at 1*C* rate and (b) discharge capacity of the Sn/C anode at different rates (the electrode was charged at *C*/10 prior to discharge at given rate).

reversible capacity originates exclusively from Sn nanoparticles and reaches ~880 mAh g^{-1} of the Sn present in the film, which is close to the theoretical value of 993 mAh g^{-1}. Interestingly, the cathodic scan of the voltammogram displays a considerable contribution from the SEI layer formation, which is much larger than expected for tin metal but smaller than is usually observed for SnO. This is also clearly visible during the galvanostatic cycles that are shown in Fig. 6b. The charge–discharging profiles display plateaus characteristic for tin but also show a significant contribution from the irreversible capacity (ca. 400 mAh g^{-1}) in the first cycle. We postulate that the irreversible capacity is mainly associated with the SEI layer formation on the carbon matrix and some small contribution from tin.

The cycling performance of the Sn/C composite anode is illustrated in Fig. 7a. The galvanostatic charge–discharge cycling was continued over 500 cycles at 1*C* rate and showed only 40% capacity fading, which presents a significant improvement if compared with the electrochemical properties of tin-based carbon composite materials reported in the literature. Veeraraghavan et al. [44] reported 35 cycles at *C*/15 and 15.8% discharge capacity loss for the Sn coated graphite materials. Carbon–tin composites produced by ball-milling showed a capacity drop from 1070 to 380 mAh g^{-1} over 20 cycles [45]. Tin–graphite materials prepared by chemical reduction of $SnCl_4$ showed the initial reversible massic capacity of 630 mAh g^{-1}, which decayed to 415 mAh g^{-1} after 25 cycles [46]. Tin nanoparticles embedded in microporous carbon matrices [48] showed a discharge capacity of 305 mAh g^{-1} after 30 cycles at *C*/10 rate whereas tin-filled carbon nano-tubes showed remarkable 844 mAh g^{-1} for 40 cycles at *C*/10 [50].

To evaluate the power capability of the Sn/C composite anode the thin-film electrode was tested at different discharge rates. Fig. 7b shows the discharge curves at *C*/25, *C*/10, *C*/5, 1*C* and 5*C* rates, which correspond to 423, 400, 386, 349 and 297 mAh g^{-1}, respectively. Such an improved rate performance as compared to 160.5 mAh g^{-1} at 2*C* for the Sn-coated graphite [44] or 200 mAh g^{-1} at 1.5*C* for Sn–Co–C alloys [51] suggests that vacuum deposition techniques to manufacture nano-structured metal–carbon thin-film anodes may indeed be a promising technology for new generation lithium-ion batteries.

The improved electrochemical behavior of the Sn/C composite anode is mainly due to the high-lithium diffusion coefficient at room temperature, high porosity of the film, and fine dispersion of Sn nanoparticles, which are embedded in the three-dimensional carbon matrix. The 3D composite design allows the accommodation of dimensional changes of Sn nanoparticles and the preservation of the structural and electronic integrity of the Sn/C electrode during cycling. The observed decrease of the reversible capacity is likely related to large tin clusters or particles, which are weakly bound to the surface of the carbon aggregates. The network-like 3D architecture of the Sn/C thin-film provides mechanical support and good electrical contact between Sn active material and the current collector. The nanometer size of Sn particles helps contain stress that arises from the expansion/contraction of the crystalline lattice of Li_xSn during charge–discharge processes and prevents particle decrepitation and the degradation of the composite anode.

4. Conclusions

In summary, we demonstrated a novel synthesis technique for the production of nanocomposite anodes for Li-ion batteries. The MPCVD co-synthesis of a nano-structured Sn/C composite thin-film described in this study presents a simple, fast, and inexpensive method for the one-step formation of electronically conductive, carbon/metal composite binderless thin films, which can be deposited on any type of substrate. The fast plasma discharge and the presence of microwave radiation accelerate the formation of sites suitable for *in situ* heterogeneous nucleation, and consequently, the growth and uniform dispersion of tin nanoparticles in the carbonaceous matrix. The electrochemical response of the Sn/C thin-film electrode in Li-ion system displays reversible charge–discharge activity, which is attributed mainly to Sn nanoparticles. The thin-film Sn/C electrodes delivered a reversible capacity of 423 and 297 mAh g^{-1} at *C*/25 and 5*C* discharge rates, respectively. A long-term cycling of the Sn/C anodes showed 40% capacity loss after 500 cycles at 1*C* rate. The improved electrochemical behavior of the Sn/C thin-film

composite anode is mainly due to the high porosity of the film and fine dispersion of Sn nanoparticles, which are embedded in the three-dimensional carbon matrix.

Acknowledgements

This work was supported by the Assistant Secretary for Energy Efficiency and Renewable Energy, Office of FreedomCAR and Vehicle Technologies of the U.S. Department of Energy under Contract No. DE-AC02-05CH11231. The authors acknowledge the assistance of the National Center for Electron Microscopy, Lawrence Berkeley Lab, which is supported by the U.S. Department of Energy under Contract No. DE-AC02-05CH11231.

References

[1] R.A. Huggins, M. Winter, J.O. Besenhard, in: J.O. Besenhard (Ed.), Handbook of Battery Materials, Wiley, New York, 1999, pp. 359–381.
[2] Y.P. Wu, E. Rahm, R. Holze, Electrochim. Acta 47 (2002) 3491–3507.
[3] M. Yoshio, H. Wang, K. Fukuda, Y. Hara, Y. Adachi, J. Electrochem. Soc. 147 (2000) 1245–1250.
[4] M. Yoshio, H. Wang, K. Fukuda, T. Umeno, T. Abe, Z. Ogumi, J. Mater. Chem. 14 (2004) 1754–1758.
[5] M. Yoshio, H. Wang, K. Fukuda, Angew. Chem. Int. Edit. 42 (2003) 4203–4206.
[6] E. Peled, C. Menachem, D. Bar-Tow, A. Melman, J. Electrochem. Soc. 143 (1996) L4–L7.
[7] H. Buqa, P. Golob, M. Winter, J.O. Besenhard, J. Power Sources 97–98 (2001) 122–125.
[8] T. Shodai, S. Okada, S. Tobishima, J. Yamaki, J. Power Sources 68 (1997) 515–518.
[9] S. Suzuki, T. Shodai, Solid State Ionics 116 (1999) 1–9.
[10] J.J. Auborn, Y.L. Barbero, J. Electrochem. Soc. 134 (1987) 638–643.
[11] E. Ferg, J. Gummow, A. de Kock, M.M. Thackeray, J. Electrochem. Soc. 141 (1994) L147–L150.
[12] T. Ohzuku, A. Ueda, N. Yamamoto, J. Electrochem. Soc. 142 (1995) 1431–1435.
[13] S.Y. Huang, L. Kavan, I. Exnar, M. Gratzel, J. Electrochem. Soc. 142 (1995) L142–L144.
[14] M.A. Cochez, J.C. Jumax, P. Lavela, J. Morales, J. Olivier-Fourcade, J.L. Tirado, J. Power Sources 62 (1996) 101–105.
[15] A. Netz, R.A. Huggins, W. Weppner, J. Power Sources 119–121 (2003) 95–100.
[16] S. Yang, P.Y. Zavalij, M.S. Whittingham, Electrochem. Commun. 5 (2003) 587–590.
[17] Y. Hamon, T. Brousse, F. Jousse, P. Topart, P. Buvat, D.M. Schleich, J. Power Sources 97–98 (2001) 185–187.
[18] K.D. Kepler, J.T. Vaughey, M.M. Thackeray, J. Power Sources 81 (1999) 383–387.
[19] M. Egashira, H. Takatsuji, S. Okada, J. Yamaki, J. Power Sources 107 (2002) 56–60.
[20] Ch.M. Burba, R. Frech, J. Electrochem. Soc. 152 (2005) A1233–A1240.
[21] H. Inoue, Abstract #228, International Meeting on Lithium Batteries, Biarritz, France, June 18–23, 2006.
[22] R.B. Lewis, A. Timmons, R.E. Mar, J.R. Dahn, J. Electrochem. Soc. 154 (2007) A213–A216.
[23] Y. Idota, T. Kubota, A. Matsufuji, Y. Maekawa, T. Miyasaka, Science 276 (1997) 1395–1397.
[24] S.H. Ng, D.I. dos Santos, S.Y. Chew, D. Wexler, J. Wang, S.X. Dou, H.K. Liu, Electrochem. Commun. 9 (2007) 915–919.
[25] A. Yu, R. Frech, J. Power Sources 104 (2002) 97–100.
[26] S. Panero, G. Savo, B. Scrosati, Electrochem. Solid State Lett. 2 (1999) 365–366.
[27] R.A. Huggins, Solid State Ionics 113–115 (1998) 57–67.
[28] M. Winter, J.O. Besenhard, Electrochim. Acta 45 (1999) 31–50, and references therein.
[29] Ou Mao, R.A. Dunlap, J.R. Dahn, J. Electrochem. Soc. 146 (1999) 405–413.
[30] Ou Mao, J.R. Dahn, J. Electrochem. Soc. 146 (1999) 423–427.
[31] Ou Mao, J.R. Dahn, J. Electrochem. Soc. 146 (1999) 414–422.
[32] L.Y. Beaulieu, J.R. Dahn, J. Electrochem. Soc. 147 (2000) 3237–3241.
[33] J.R. Dahn, R.E. Mar, Alyaa Abouzeid, J. Electrochem. Soc. 153 (2006) A361–A367.
[34] J.O. Besenhard, M. Wachtler, M. Winter, R. Andreaus, I. Rom, W. Sitte, J. Power Sources 81–82 (1999) 268–272.
[35] L.Y. Beaulieu, K.C. Hewitt, R.L. Turner, A. Bonakdarpour, A.A. Abdo, L. Christensen, K.W. Eberman, L.J. Krause, J.R. Dahn, J. Electrochem. Soc. 150 (2003) A149–A156.
[36] T.D. Hatchard, J.M. Topple, M.D. Fleischauer, J.R. Dahn, Electrochem. Solid State Lett. 6 (2003) A129–A132.
[37] T.D. Hatchard, M.N. Obrovac, J.R. Dahn, J. Electrochem. Soc. 153 (2006) A282–A287.
[38] J.R. Dahn, R.L. Turner, Ou Mao, R.A. Dunlap, A.E. George, M.M. Buckett, D.J. McClure, L.J. Krause, Thin Solid Films 408 (2002) 111–122.
[39] A. Bonakdarpour, K.C. Hewitt, T.D. Hatchard, M.D. Fleischauer, J.R. Dahn, Thin Solid Films 440 (2003) 11–18.
[40] T.D. Hatchard, J.R. Dahn, S. Trussler, M. Fleischauer, A. Bonakdarpour, J.R. Mueller-Neuhaus, K.C. Hewitt, Thin Solid Films 443 (2003) 144–155.
[41] G.M. Ehrlich, C. Durand, X. Chen, T.A. Hugener, F. Spiess, S.L. Suib, J. Electrochem. Soc. 147 (2000) 886–891.
[42] L. Yuan, Z.P. Guo, K. Konstantinov, H.K. Liu, S.X. Dou, J. Power Sources 159 (2006) 345–348.
[43] I.A. Courtney, W.R. McKinnon, J.R. Dahn, J. Electrochem. Soc. 146 (1999) 59–68.
[44] B. Veeraraghavan, A. Durairajan, B. Haran, B. Popov, R. Guidotti, J. Electrochem. Soc. 149 (2002) A675–A681.
[45] G.X. Wang, J. Ahn, M.J. Lindsay, L. Sun, D.H. Bradhurst, S.X. Dou, H.K. Liu, J. Power Sources 97–98 (2001) 211–215.
[46] L. Balan, R. Schneider, P. Willmann, D. Billaud, J. Power Sources 161 (2006) 587–593.
[47] W.A. Ulus, Yu. Rosenberg, L. Burstein, E. Peled, J. Electrochem. Soc. 149 (2002) A635–A643.
[48] I. Grigoriants, A. Soffer, G. Salitra, D. Aurbach, J. Power Sources 146 (2005) 185–189.
[49] L. Yuan, K. Konstantinov, G.X. Wang, H.K. Liu, S.X. Dou, J. Power Sources 146 (2005) 180–184.
[50] T. Prem Kumar, R. Ramesh, Y.Y. Lin, G. Ting-Kuo Fey, Electrochem. Commun. 6 (2004) 520–525.
[51] J. Hassoun, G. Mulas, S. Panero, B. Scrosati, J. Power Sources 9 (2007) 2075–2081.
[52] W.H. Lee, H.C. Son, H.S. Moon, Y.I. Kim, S.H. Sung, J.Y. Kim, J.G. Lee, J.W. Park, J. Power Sources 89 (2000) 102–105.
[53] N. Kuwata, J. Kawamura, K. Toribami, T. Hattori, N. Sata, Electrochem. Commun. 6 (2004) 417–421.
[54] N. Li, Ch.R. Martin, J. Electrochem. Soc. 148 (2001) A164–A170.
[55] P. Limthongkul, H. Wang, E. Jud, Y. Chiang, J. Electrochem. Soc. 149 (2002) A1237.
[56] G.J. Li, S. Kawi, Mater. Lett. 34 (1998) 99–102.
[57] D. Aurbach, A. Nimberger, B. Markovsky, E. Levi, E. Sominski, A. Gedanken, Chem. Mater. 14 (2002) 4155–4166.
[58] Y. Wang, J.Y. Lee, H.C. Zeng, Chem. Mater. 17 (2005) 3899–3907.
[59] M. Marcinek, X. Song, R. Kostecki, Electrochem. Commun. 9 (2007) 1739–1743.
[60] W. Kraus, G. Noltze, Powder Cell for Windows, 2.4, Federal Institute for Materials Research and Testing, Berlin, Germany, 2000.
[61] J.I. Goldstein, Ch.E. Lyman, D.E. Newbury, E. Lifshin, P. Echlin, L. Sawyer, D.C. Joy, J.R. Michael, Scanning Electron Microscopy and X-Ray Microanalysis, 3rd ed., Springer, 2003, p. 361.
[62] F. Tuinstra, J.L. Koenig, J. Chem. Phys. 53 (1970) 1126–1130.
[63] R. Saito, A. Jorio, A.G. Souza Filho, G. Dresselhaus, M.S. Dresselhaus, M.A. Pimenta, Phys. Rev. Lett. 88 (2002) 027401–027404.
[64] A.C. Ferrari, J. Robertson, Phys. Rev. B 61 (2000) 14095–14107.

[65] M.A. Pimenta, G. Dresselhaus, M.S. Dresselhaus, L.G. Cancado, A. Jorio, R. Saito, Phys. Chem. Chem. Phys. 9 (2007) 1276–1291.
[66] R.C. Mani, M.K. Sunkara, R.P. Baldwin, J. Gullapalli, J.A. Chaney, G. Bhimarasetti, J.M. Cowley, A.M. Rao, R. Raod, J. Electrochem. Soc. 152 (2005) E154–E159.
[67] A.D. Lueking, H.R. Gutierrez, D.A. Fonseca, E. Dickey, Carbon 45 (2007) 751–759, and references therein.
[68] K. Kinoshita (Ed.), Carbon-Electrochemical and Physicochemical Properties, John Wiley and Sons, New York, 1988, and references therein.